scientific reports

Check for updates

OPEN

Characterization of post-inflammatory irritable bowel syndrome animal model following acute colitis recovery

Eui Sun Jeong[1], Hye-Kyung Jung[1]✉, Euno Choi[2], Kyeongeui Yun[3], Ayoung Lee[4] & Yong Sung Kim[5]

Irritable bowel syndrome (IBS) is a prevalent disorder with an unclear pathophysiology. This study aimed to investigate the features of dextran sulfate sodium (DSS)-induced low-grade inflammation using murine models of acute severe colitis (acute model) and chronic mild repeated colitis (chronic model), with potential implications for IBS research. The acute model was induced with 3% DSS for 5 days, followed by a 12-week recovery period. The chronic model involved administration of 0.5% DSS for 5 days, followed by a 5-day resting period, repeated thrice. We conducted comparative analyses to assess inflammation severity, intestinal motility, permeability, visceral hypersensitivity, and microbiome composition. In the acute model, mild leukocyte infiltration was observed, colonic transit time shortened at 12 weeks ($P < 0.001$), occludin expression decreased ($P = 0.041$), inflammatory cytokines, and transient receptor potential vanilloid 1 was upregulated in colonic mucosa ($P < 0.050$). In the chronic model, only mild inflammatory changes were noted. Microbiota analysis in the acute model revealed differences in microbial abundance and compositions ($P = 0.001$). The acute model demonstrated low-grade inflammation that caused gut dysmotility, altered permeability, and increased visceral hypersensitivity with notable microbial composition changes, potentially relevant to IBS phenotypes.

Keywords Irritable bowel syndrome, Murine model, Dextran sulfate sodium, Low-grade inflammation, Dysmotility, Microbiome

Irritable bowel syndrome (IBS) is a prevalent functional gastrointestinal disorder characterized by recurring abdominal pain associated with defecation or changes in bowel habits with no evidence of abnormalities in digestive organs[1]. The prevalence of IBS has been estimated to exceed 10% of the global population[1], underscoring its significant medical concern. IBS substantially affects the quality of life of patients and places a considerable burden on the healthcare system[2]. IBS is a multifactorial disease and the precise pathophysiology is unclear[3,4]. The pathogenesis of IBS has focused on abnormalities in visceral hypersensitivity, motility, brain-gut interaction, and psychosocial distress, and more recently, altered immune activation, changes of gut permeability and microbiome have been demonstrated in a subset of IBS patients[3,4]. Additionally, the influence of diet and nutritional components further contributes to the intricate dynamics of IBS.

Research on developing and validating animal models based on IBS pathophysiology has gained interest for the effective management of IBS[3]. Various animal models have been developed to study IBS, among which the stress-induced chronic visceral pain model is the most commonly used. However, these models possess limitations in fully replicating the complexity of human IBS. Wang et al.[5] proposed a rodent model involving central stimulation induced by water avoidance stress, restraint stress, and neonatal-maternal separation. Additionally, Moloney et al.[6] described two pain models: early-life stress-induced visceral pain using a maternal separation stress model and adult stress-induced visceral pain using acute or chronic water avoidance stress. Although these IBS animal models have contributed to the understanding of psychosocial or life-threatening

[1]Department of Internal Medicine, College of Medicine, Ewha Womans University, Seoul, Korea. [2]Department of Pathology, College of Medicine, Ewha Womans University, Seoul, Korea. [3]HuNBiome Co., Ltd., R&D Center, Seoul, Korea. [4]Department of Internal Medicine, College of Medicine, Korea University, Ansan, Gyeonggi-do, Korea. [5]Digestive Disease Research Institute, College of Medicine, Wonkwang University, Iksan, Jeonlabuk-do, Korea. ✉email: junghk@ewha.ac.kr

stress, there is a need for versatile methods that can effectively address the complexities of IBS modeling while avoiding complex experimental setups and equipment, and adhering to animal research ethics.

Another IBS model was the post-infectious induced IBS model. Long et al.[7] investigated visceral hyperalgesia and colonic muscle hypercontractility in IBS mice models induced by acute or chronic *Trichinella spiralis* infection. Piccione et al.[8] analyzed an increase in interleukin (IL)-1β and tumor necrosis factor (TNF)-α among mucosal cytokines in IBS patients and demonstrated this in a dextran sulfate sodium (DSS)-induced *in vitro* study. Similar to its application in inflammatory bowel disease (IBD), the post-inflammatory model emerges as a potential candidate for an IBS animal model, complementing those induced by psychological or life-threatening stress. Clinical symptoms overlap in patients with IBD who also present IBS-like symptoms[9]. DSS-induced colitis mouse model has been widely used in IBD studies due to its ease of administration[5,10]; however, the exploration of experimental modeling specifically targeting low-grade inflammation related to IBS remains limited. Kodani et al.[11] analyzed gastrointestinal motility and macrophage/mast cell distribution during healing after induction of acute colitis with 2% DSS. However, similar to previous post-infectious IBS models, this study only analyzed changes following acute colitis, focusing on motility while not considering various other pathophysiological aspects of IBS, such as changes in visceral hypersensitivity, intestinal permeability, or microbial composition.

Therefore, this study aimed to investigate DSS-induced low-grade inflammation following acute severe colitis or chronic mild repeated colitis and evaluate its features, including gut dysmotility, permeability changes, visceral hypersensitivity, and microbiome alterations, which may resemble IBS-like phenotypes in a simple and efficient manner.

Materials and methods

Experimental design

Seven-week-old C57BL/6 male mice (Orient Bio Co., Ltd.*, Seongnam, Gyeonggi, Korea) were used in this study for IBS model induction. The mice were acclimated for 7 days at the Medical Research Center's facility before experimentation. Mice were housed individually in standardized environmental conditions at 23 ± 2 °C with 50–55% humidity and were allowed to feed food and drink ad libitum. The study protocol was approved by the Ethics Committee for Animal Research (EUM19-0456) and followed the ARRIVE 2.0 guidelines. Experimental procedures and results were conducted in accordance with regulations and guidelines.

The mice were divided into two groups to induce the post-inflammatory IBS modeling: an acute severe colitis recovery IBS model (acute model) and a chronic mild repeated colitis IBS model (chronic model) (Fig. 1). For acute model, mice ($n = 10$) were administered with 3% DSS (MP biochemical*, Irvine, CA, USA) for 5 days, followed by a 12-week recovery period. During the recovery period, mice were given free access to food and water. The traditional IBD model involved a chronic model in which mice ($n = 10$) were orally administered with DSS for 5 days, followed by a recovery period of drinking water for the next 5 days, repeated for 3 cycles. To induce low-grade inflammation without causing gross mucosal damage, preliminary experiments were conducted to find an appropriate concentration of DSS, including 0.5%, 1.0%, and 1.5% for chronic models ($n = 3$ for each group). Body weight changes, stool consistency, and gross bleeding were measured by the same observer every 7 days in the acute model and 3 days in the chronic model to assess disease activity, and the disease activity index (DAI) was calculated by adding the changes in body weight, stool consistency, and gross bleeding (Supplementary Table S1)[12].

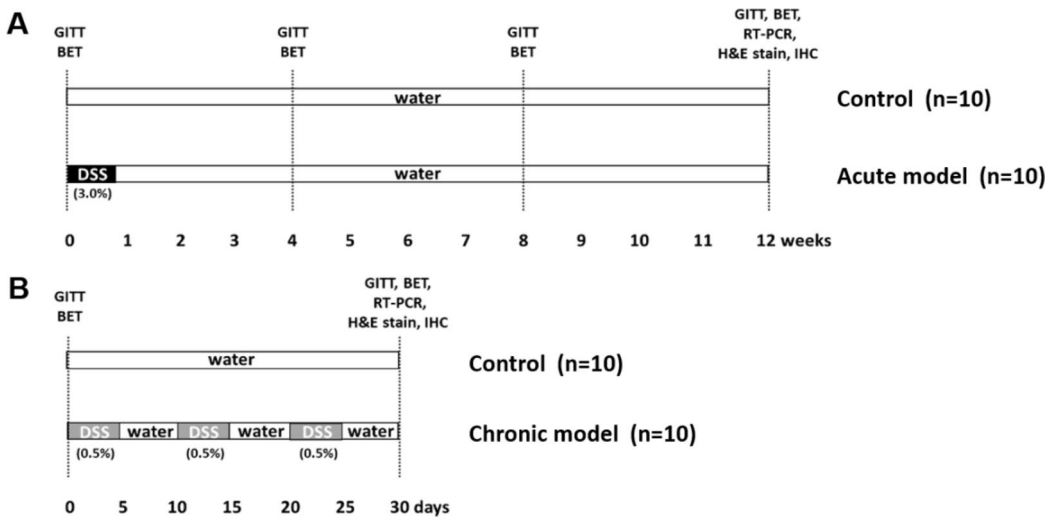

Fig. 1. Experimental design for post-inflammatory IBS animal model. (**A**) Acute severe colitis recovery IBS model (acute model, $n = 10$), 3% DSS was administered for 5 days followed by a 12-week recovery period. (**B**) Chronic mild repeated colitis IBS model (chronic model, $n = 10$), 0.5% DSS was administered for 5 days, followed by a 5-day resting period, repeated three times over 30 days. *IBS* irritable bowel syndrome, *DSS* dextran sulfate sodium, *GITT* gastrointestinal transit time, *BET* bead expulsion test, *RT-PCR* real-time polymerase chain reaction, *H&E stain* hematoxylin-eosin stain, *IHC* immunohistochemistry.

After completing the experiment in each model, all mice were euthanized through CO_2 asphyxiation after overnight fasting. After euthanasia, the entire colon was dissected from the cecum, and the total length was measured. Whole colon tissue was divided into proximal and distal sections, and then tissue from each section was split and analyzed by real-time polymerase chain reaction (RT-PCR), histopathology, and immunohistochemistry (IHC).

Analysis of intestinal transit time

We used the gastrointestinal transit time (GITT) and the bead expulsion test to determine the intestinal transit time. For both techniques, we measured transit time before DSS administration and then every 4 weeks for the acute model and 30 days for the chronic model, respectively. Mice were housed individually to measure the GITT. A 6% solution of carmine red (natural red 4; Sigma Aldrich®, St. Louis, MO, USA), a non-absorbable dye, was administered through a 21-gauge gavage in 0.3 mL of 0.5% methylcellulose solution (Sigma Aldrich®). Following administration, mice were placed in a cage, the floors of which were lined with white paper to facilitate the carmine-red coloration of their feces. T_0 represented the time at which the carmine red solution was gavaged and the time it took for the expulsion of the first red fecal pellet was assessed[13]. In GITT measurements, closed-circuit television (CCTV) was employed as an auxiliary tool for more objective and accurate measurement.

In the existing murine animal model, a bead expulsion test was a commonly used method to measure distal colonic transit time[14]. The distal colonic transit time was defined as the time between the bead insertion into the distal colon and its expulsion. Briefly, similar to previous studies, we dipped a single 2 mm bead into the lubricating gel, gently inserted it, and measured the time to expulsion.

RT-PCR analysis of inflammatory cytokines and permeability markers

The mRNA expression of inflammatory cytokines in the mice colon, including IL-1β, IL-6, IL-17, and TNF-α was measured. We assessed the mRNA expression of occludin, zonular occludens (ZO)-1, claudin-1, and claudin-4 using RT-PCR[15] to assess the expression of the tight junction proteins in the IBS model.

RT-PCR was performed on proximal and distal colon sections. The separated colon tissue was immediately frozen at − 70 °C in a cryogenic freezer. Total RNA was isolated from colon tissue using the TRIzol reagent (Ambion®, Waltham, MA, USA). After adding chloroform (Sigma Aldrich®), the extracted total RNA was centrifuged at 12,000 rpm for 10 min at 4 °C. The supernatants were centrifuged for 10 min at 12,000 rpm at 4 °C with isopropanol (Sigma Aldrich®). After 75% ethanol wash, the pellet was solubilized with nuclease-free water and quantified using nano drops. RNA (2 µg) was reverse-transcribed in the mixture of oligo dT primers (0.5 µg), 200 units of Molony-Murine leukemia virus reverse transcriptase (Promega®, Fitchburg, WI, USA), 5x RT buffer, dNTPs (2 nM), and 25 units of RNasin ribonuclease inhibitor (Promega®) at 42 ℃ for 60 min. The RT-PCR was conducted on 7000 Real-time PCR systems (Applied Biosystems®, Waltham, MA, USA) with 2X Power SYBR Green PCR Master mix (Applied Biosystems®), 0.1 µg cDNA, and each primer set (Macrogen®, Seoul, Korea; Supplementary Table S2) over 40 cycles (95 ℃ for 15 s and 60 ℃ for 60 s) following pre-denature at 95 ℃ for 10 min. The relative expression of the target genes was assessed using the comparative Ct method, and glyceraldehyde-3-phosphate dehydrogenase was used as an internal control.

Histopathological analysis

Histopathological examination was conducted by a single pathologist, and colon tissues were fixed in 10% formalin, followed by paraffin sectioning and hematoxylin-eosin (H&E) staining. Each colon tissue was stained with H&E and analyzed in three categories for histological evaluations: (i) inflammatory cell infiltrate, (ii) epithelial changes, and (iii) mucosal architecture. According to the criteria in histomorphological scores for intestinal inflammation in mouse models (Supplementary Table S3), each category was calculated with a score value ranging from 1 to 5[16].

Immunohistochemistry analysis

IHC analysis was performed, focusing on neuroinflammatory markers. Tissue samples were fixed in 4% paraformaldehyde in phosphate-buffered saline (pH 7.4), embedded in paraffin, and sectioned for IHC analysis. After deparaffinization and rehydration, antigen retrieval was performed by incubating the sections in citrate buffer (0.01 mmol/L, pH 6.0) and heating them in a microwave oven (720 W) for 15 min. Endogenous peroxidase was blocked by treating the sections in 0.3% hydrogen peroxide for 30 min at room temperature. Next, sections were incubated for 3 h at room temperature with specific antibodies: rabbit polyclonal transient receptor potential vanilloid 1 (TRPV1) antibody (Invitrogen®, Waltham, USA), recombinant rabbit monoclonal tropomyosin receptor kinase A (TrkA) antibody (Invitrogen®), mouse monoclonal substance P antibody (Santa Cruz®, Dallas, TX, USA), rabbit monoclonal S-100 antibody (Leika®, Wetzlar, Germany), and mouse monoclonal neuron-specific enolase (NSE) antibody (Leika®) as visceral hypersensitivity markers. The sections were then incubated with horseradish peroxidase-conjugated goat anti-rabbit secondary antibodies for 30 min. The sections were then stained with 3,3-diaminobenzidine solution, followed by counterstaining with hematoxylin for nuclei labeling[17]. Immunopositive cells were counted using the Image J program (National Institutes of Health, Bethesda, MD, USA) in a 200 µm stretch of well-oriented entire colon epithelium sections at five randomly selective fields for each antibody. The average and standard deviation were subsequently calculated[11].

Microbiome analysis

We performed a microbiome analysis on the acute model selected as the IBS model based on comprehensive results. For microbiome analysis, intraluminal feces were collected from cecum of sacrificed mice and immediately frozen at − 80 ℃. Microbial genomic DNA was extracted using QIAamp PowerFecal Pro DNA Kit (Qiagen®, Hilden, North Rhine-Westphalia, Germany), following the recommended protocols. The quality of all extracted bacterial genomic

DNA was assessed using the Qubit 4 (ThermoFisher Scientific®, Waltham, MA, USA). The extracted mitochondrial DNA samples were stored at 4°C until further processing. The DNA sequencing library targeting the V3 and V4 hypervariable regions of 16S ribosomal RNA was constructed according to the sequencing library preparation protocol (Illumina®, San Diego, CA, USA) using specific universal primers (Illumina 16S forward 341F primer, 5′-TCGTCGGCAGCGTCAGATGTGTATAAGAGACAGCCTACGGGNGGCWGCAG-3′ and reverse 805R primer, 5′-GTCTCGTGGGCTCGGAGATGTGTATAAGAGACAG GACTACHVGGGTATCTAATCC-3′)[18]. PCR was carried out using KAPA HiFi HotStart ReadyMix (Kapa Biosystems®, Wilmington, MA, USA), followed by purification of the PCR product with AMPure XP beads (Beckman Coulter Genomics®, Brea, CA, USA). An additional PCR amplification was performed to introduce the Illumina adapter and multiplex indices using the Nextera XD Index (Illumina®). The final PCR products were purified once again using the AMPure XP beads. The prepared library was then sequenced using the Miseq system (Illumina®) with 300 bp paired-end reads.

The gut microbiome data was analyzed using the QIIME2 pipeline plugin (2022.08)[19]. Before implementing DADA2 (Divisive Amplicon Denoising Algorithm 2) in QIIME2, Figaro was used to determine optimal options based on sequence quality[20].

Amplicon sequence variants (ASVs) were obtained through the denoising step in the DADA2 algorithm. The ASVs were subjected to bacterial classification using a Naïve Bayes classifier based on targeted hypervariable reads extracted from the SILVA 138v 99% rRNA database to improve accuracy. Subsequently, various features annotated with Archaea, Eukaryotes, Mitochondria, or Chloroplasts were removed. The selected bacterial features were employed for the construction of a phylogeny tree using the align-to-tree-mafft-fasttree plugin, and taxonomy composition was determined. These features were rarefied at a specified depth and utilized for the analysis of alpha diversity, including Observed Features, Chao1 Index, Shannon's Index, Simpson's Index, and Pielou's Evenness, as well as beta diversity, encompassing Bray-Curtis and Unweighted UniFrac metrics[21].

Statistical analysis

Statistical Package for the Social Sciences (SPSS) program, version 25.0 software (SPSS Inc.®, Chicago, IL, USA) was used for all statistical analysis. The mean ± standard deviation values were used for each analysis. Comparisons of values between the models were tested using the nonparametric Kruskal–Wallis test. Graphical representations were generated using GraphPad Prism software version 8 (GraphPad Software Inc.®, La Jolla, CA, USA). A P-value of < 0.050 was considered statistically significant.

For microbiome analysis, statistical significance in group comparisons for α-diversity and taxonomy composition was evaluated using the Mann-Whitney U-test (Wilcoxon Rank-sum test) in R through the 'ggpubr' package. To confirm the similarity between groups in distance matrices from β-diversity, principal coordinate analysis and permutational analysis of variance with 999 permutations were performed using the 'Vegan' and 'Adonis' packages in R. Additionally, linear discriminant analysis effect size (LEfSe) was calculated and features with a linear discriminant analysis score ≥ 2.0 were considered significant within each group[22].

Results

Changes in the DAI of the IBS models

In the acute model, the body weight decreased by 10.1 ± 3.1% in the two weeks, then gradually increased and recovered in four weeks. The average DAI score was elevated at two weeks after DSS administration (6.8 ± 1.1), and no disease activity was observed after four weeks (Fig. 2A).

In the chronic model, body weight increased in the control, 0.5%, and 1.0% DSS groups but decreased by 3.2 ± 7.6% in the 1.5% DSS group. Gross bleeding was observed only in the 1.0% DSS group (0.3 ± 0.6), whereas diarrhea or loose stool was observed in the 1.0%, 1.5%, and 0.5% DSS groups. The DAI scores were higher in the 1.0% and 1.5% DSS groups (5.3 ± 1.5 and 4.5 ± 2.1, respectively) than in the 0.5% DSS group (1.0 ± 0.0; Fig. 2B).

Changes in colon length in the IBS models

The colon length did not differ between the acute model and the control (99.5 ± 7.9 mm vs. 103.0 ± 9.6 mm, $P = 0.420$). In the chronic model, the colon length in the 0.5% DSS group did not show significant differences from the control (92.9 ± 6.6 mm vs. 103.0 ± 9.6 mm, $P = 0.264$); however, those in the 1.0% and 1.5% DSS groups ($P = 0.009$ and $P = 0.036$) decreased significantly (Fig. 2C,D).

Changes in colon transit time in the IBS models

In the acute model, GITT slowed compared to the control group up to 8 weeks after colitis induction but significantly accelerated by 12 weeks (146.9 ± 40.2 min vs. 221.0 ± 25.0 min, $P < 0.001$; Fig. 3A). In the chronic model, no significant change in transit time was observed compared to the control after 30 days (157.0 ± 33.2 min vs. 151.2 ± 38.4 min, $P = 0.937$; Fig. 3C). Moreover, no significant difference was observed in distal colon transit by bead expulsion test between the IBS models and the controls (Fig. 3B,D). GITT measurements were accurately compared using CCTV (Fig. 3E).

Expression of inflammatory cytokine mRNAs in the IBS models

In the proximal colon of the acute model, the mean mRNA expression of IL-1β and IL-17 were increased compared to those in the controls (2.0 ± 0.7 vs. 1.2 ± 0.8, $P = 0.034$ for IL-1β; Fig. 4A, 2.5 ± 2.9 vs. 1.0 ± 0.7, $P = 0.041$ for IL-17; Fig. 4B). In the distal colon of the acute model, the mean mRNA expression of IL-1β, IL-17, and TNF-α showed a significant increase compared to those in the controls (2.1 ± 1.4 vs. 1.0 ± 0.5, $P = 0.049$ for IL-1β; Fig. 4E, 2.9 ± 3.3 vs. 1.1 ± 0.8, $P = 0.028$ for IL-17; Fig. 4F, and 2.0 ± 1.1 vs. 1.0 ± 0.3, $P = 0.018$ for TNF-α; Fig. 4G).

In the distal colon of the chronic model, a significant increase in the mean mRNA expression of IL-17 compared to that in the controls (2.3 ± 1.7 vs. 1.1 ± 0.5, $P = 0.026$; Fig. 4F). However, no remarkable increase

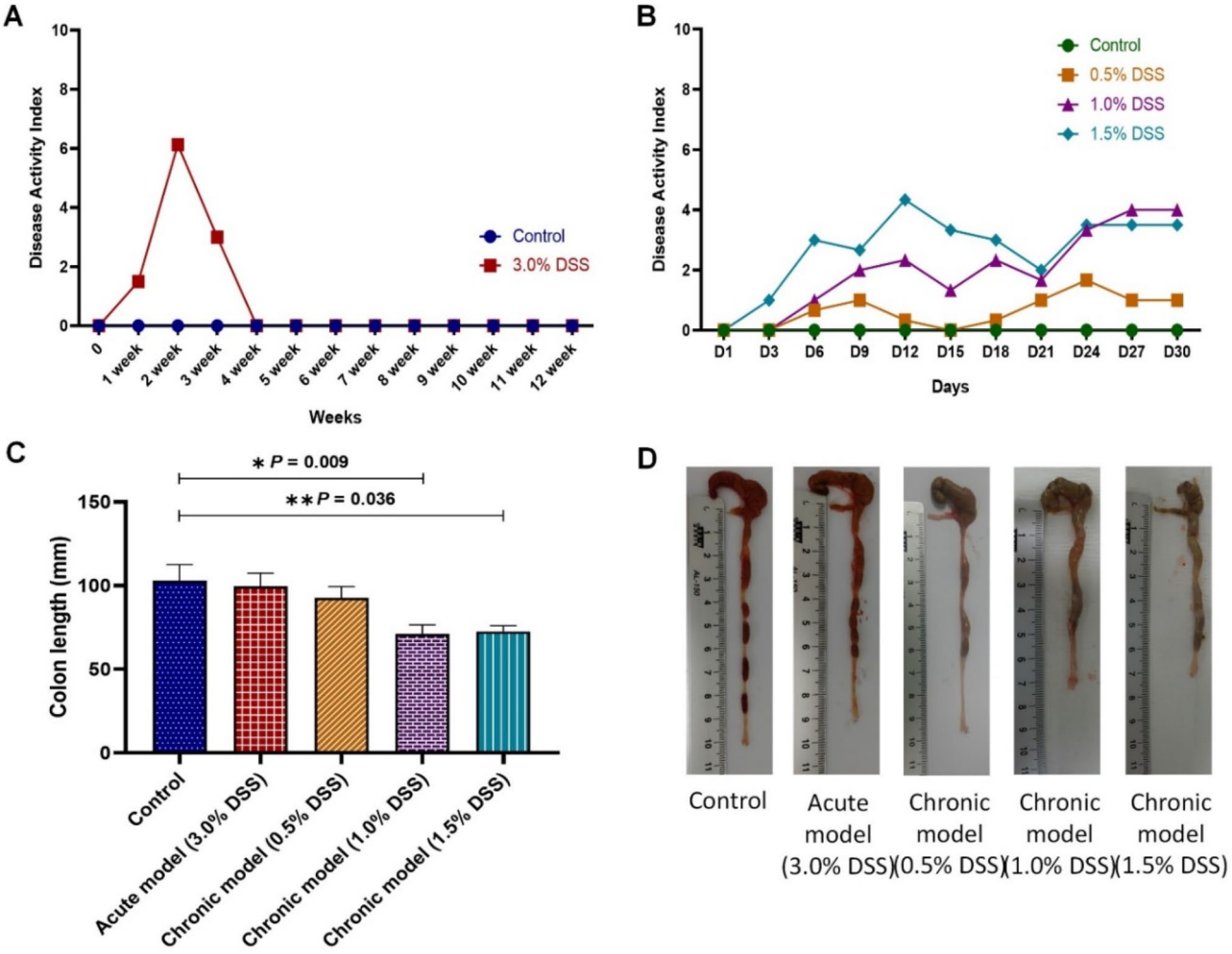

Fig. 2. Changes in the DAI and colon length of the irritable bowel syndrome models. (**A**) The average DAI comparison between the control and the acute model with weeks on the X-axis and DAI scores on the Y-axis. Each group consisted of 10 mice (Control: $n = 10$, Acute model: $n = 10$) (**B**) In preliminary experiments, DAI comparison between the control and different chronic models. Each group consisted of 3 mice (Control: $n = 3$, 0.5% DSS: $n = 3$, 1.0% DSS: $n = 3$, 1.5% DSS: $n = 3$). (**C**) Comparison of average colon length among the control, the acute model, and the chronic models. Shortening of the colon is an indicator of inflammation and tissue damage. (**D**) Photographs of colons from the control, the acute model, and the chronic models, demonstrating differences in colon length and appearance. *DAI* disease activity index.

in the expression of the inflammatory cytokines was observed in the proximal colon of the chronic model compared to that in the controls (Fig. 4A–D).

Expression of tight Junction protein coding mRNAs in the IBS models

Compared to that in the controls, the expression of occludin mRNA in the proximal colon was only significantly decreased in the acute model (0.9 ± 0.4 vs. 1.5 ± 0.8, $P = 0.041$; Fig. 4D). In the distal colon, there was no difference between the two models (Fig. 4H). In both models, the expression of ZO-1, claudin-1, and claudin-4 mRNAs did not differ from their expression in controls (Supplementary Fig. S1A–F).

Histopathological evaluation in the IBS models

The inflammatory severity and extent in colon tissue were evaluated using H&E stain (Supplementary Fig. S2). In both models, the colon tissue was observed to be grossly normal. The mild leukocyte infiltration was mainly observed in the distal colon of both models.

Expression of neuroinflammatory markers in the IBS models

In both the acute model and the control, the expression of TRPV1 and TrkA in the colonic epithelium was observed (Fig. 5A–C). Scattered and weak IHC staining was observed on the basolateral membrane of epithelial cells, while inflammatory cells in the epithelium and lamina propria showed relatively strong TRPV1 and TrkA expressions in the acute model (Fig. 5C). Quantitative analysis using the Image J program revealed increased

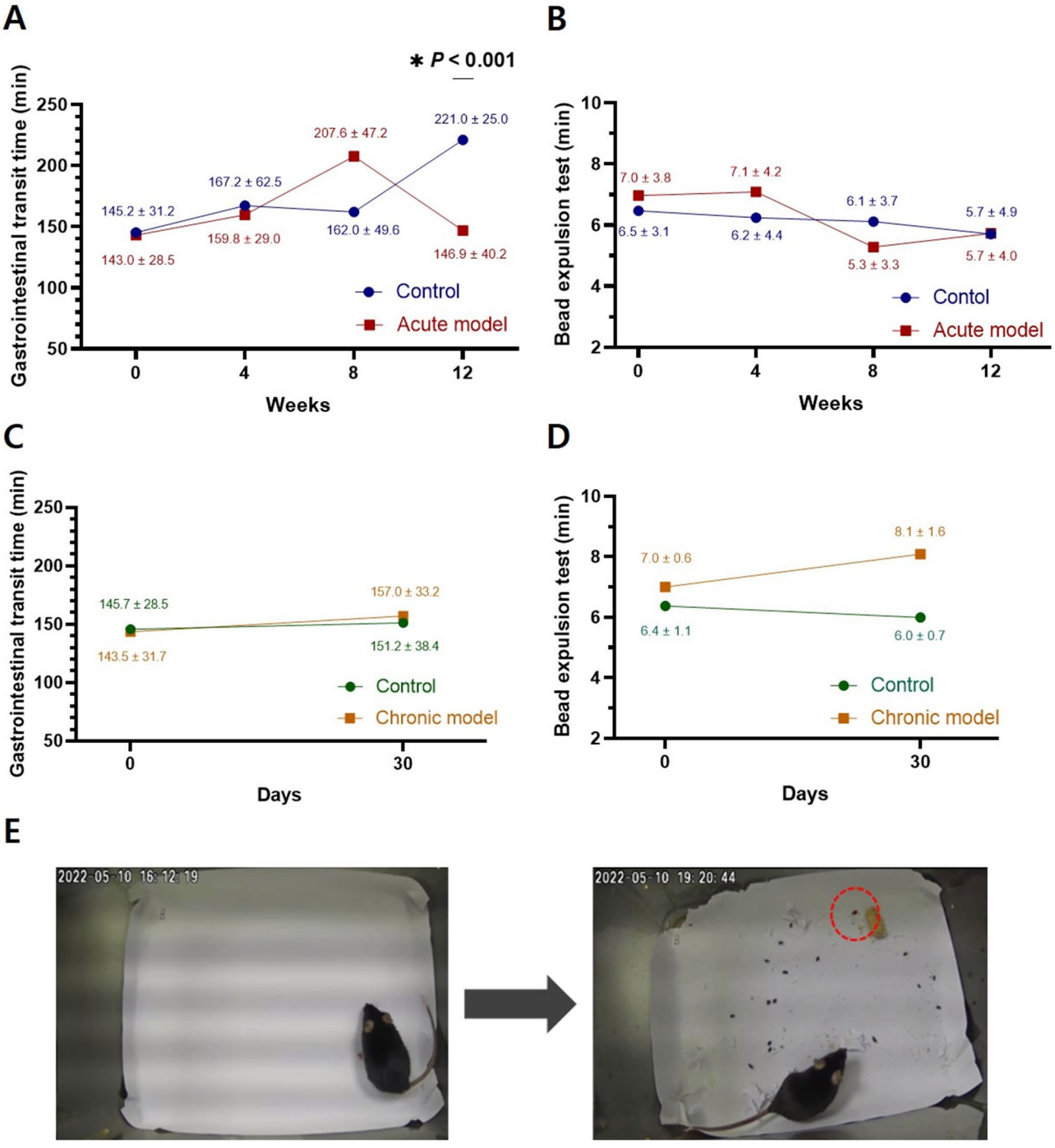

Fig. 3. Changes in colon transit time of the irritable bowel syndrome models. (**A**) Comparison of GITT between the control and the acute model. GITT was measured as the time taken for carmine red dye to travel through the gastrointestinal tract. (**B**) Comparison of BET between the control and the acute model. BET measures the time taken for a bead inserted into the distal colon to be expelled. (**C**) Comparison of GITT between the control and the chronic model. (**D**) Comparison of BET between the control and the chronic model. (**E**) Representative images from closed-circuit television used to monitor GITT. Left image shows the time of carmine red administration (T_0), and the right image shows the first appearance of carmine red-colored stool (indicated by red dots circle). Each group consisted of 10 mice (Control: $n = 10$, Acute model: $n = 10$, Chronic model: $n = 10$). Each analytic value in graphs (**A**–**D**) is expressed as mean ± standard deviation. *GITT* gastrointestinal transit time, *BET* bead expulsion test.

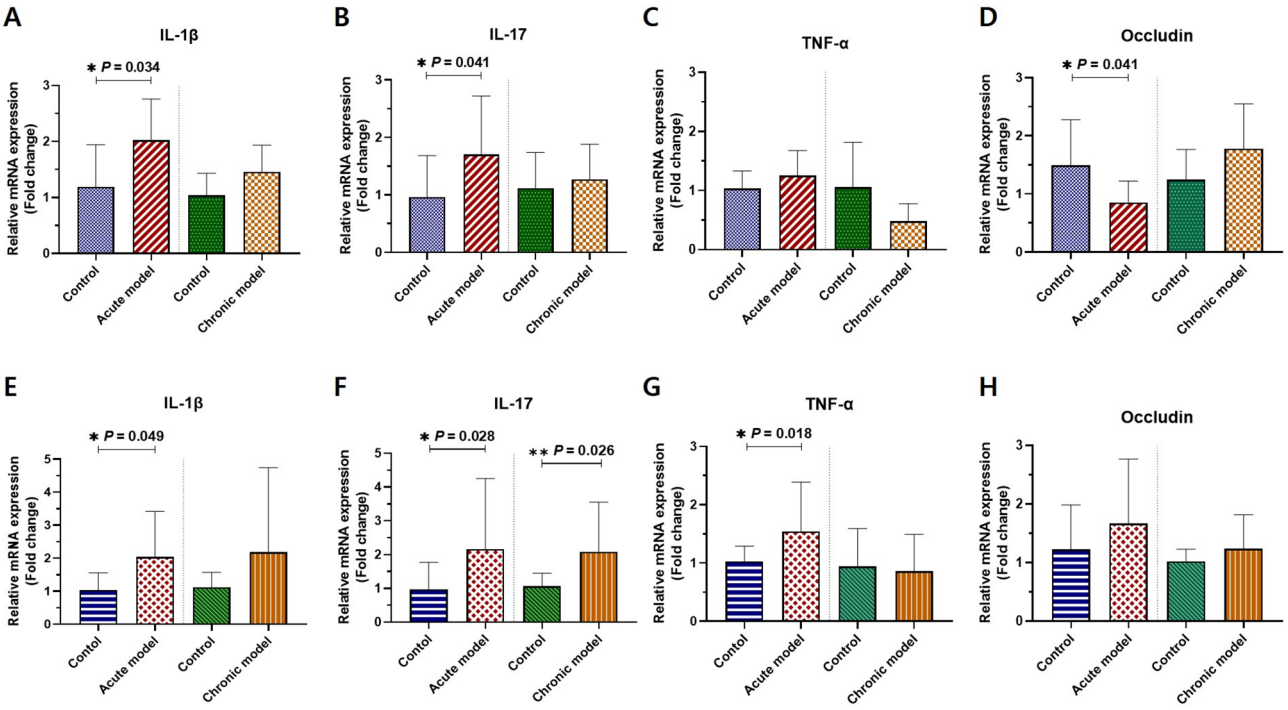

Fig. 4. mRNA expression of genes encoding inflammatory cytokines and tight junction proteins in the proximal and the distal colons of the irritable bowel syndrome models. (**A**–**D**) Mean mRNA expression values of IL-1β (**A**), IL-17 (**B**), TNF-α (**C**), and occludin (**D**) in the proximal colon of both models. In the acute model, elevated levels of IL-1β, IL-17, and TNF-α indicate increased inflammation, while decreased occludin suggests compromised intestinal barrier function. (**E**–**H**) Mean mRNA expression values of IL-1β (**E**), IL-17 (**F**), TNF-α (**G**), and occludin (**H**) in the distal colon of both models. Each group consisted of 10 mice (Control: $n = 10$, Acute model: $n = 10$, Chronic model: $n = 10$). mRNA expression was quantified using the comparative Ct method with glyceraldehyde-3-phosphate dehydrogenase as the internal control. *IL* interleukin, *TNF* tumor necrosis factor.

immunopositivity in TRPV1 and TrkA in the acute model compared to that in the controls (412.2 ± 80.1 vs. 72.6 ± 21.4, $P = 0.008$ for TRPV1 and 392.6 ± 63.4 vs. 96.2 ± 14.2, $P = 0.008$ for TrkA) (Fig. 5A,B). However, immunopositivity of substance P, S100, and NSE was rarely detected in the acute model (Supplementary Fig. S3A–C).

In contrast, in the chronic model, none of the markers showed significant differences in expression compared to controls (64.6 ± 13.6 vs. 48.4 ± 10.8, $P = 0.095$ for TRPV1; 67.2 ± 16.5 vs. 75.2 ± 11.8, $P = 0.310$ for TrkA) (Fig. 5A,B and Supplementary Fig. S3).

Comparative analysis of microbiomes in control and the IBS model

The alpha-diversity analysis, encompassing Observed features, Chao1 index, Shannon's index, Simpson's index, and Pielou's evenness, did not reveal a significant difference in the level of diversity within individual samples between the acute model and the controls ($P > 0.050$; Fig. 6A). However, the beta-diversity analysis between the two groups indicated notable differences in both Bray-Curtis dissimilarity ($P = 0.001$) and Unweighted UniFrac dissimilarity ($P = 0.001$), reflecting distinct microbial composition and dissimilarity (Fig. 6B). At the genus level, 16 genera exhibited statistically significant differences between the two groups ($P < 0.050$). LFfSe analysis revealed a higher abundance of *Lachnospiraceae*, *Erysipelatoclostridium*, *[Eubacterium] xylanophilum*, *Colidextribacter*, *Ruminococcaceae UBA1819*, *Marvinbryantia*, *Anaerotruncus*, and *Turicibacter* in the acute model compared to that in the control. Conversely, *Clostridium sensu stricto 1*, *Ruminococcus*, *Bifidobacterium*, *Clostridia UCG-014*, *Anaeroplasma*, *[Eubacterium] fissicatena*, and *Romboutstia* exhibited a relatively higher abundance in the control group than that in the acute model (Fig. 7). These results showed no difference in the alpha diversity between the acute model and the control; however, noticeable changes in microbial composition were observed in the acute model.

Discussion

In this study, we characterized DSS-induced low-grade inflammation using a recovery model following acute severe colitis. The findings revealed notable physiological changes, including altered gut motility, increased expression of neuroinflammatory markers, and changes in microbial composition, without evident clinical or histological manifestations of colonic damage. These features may resemble IBS-related phenotypes and provide insights for future research into post-inflammatory mechanisms relevant to IBS.

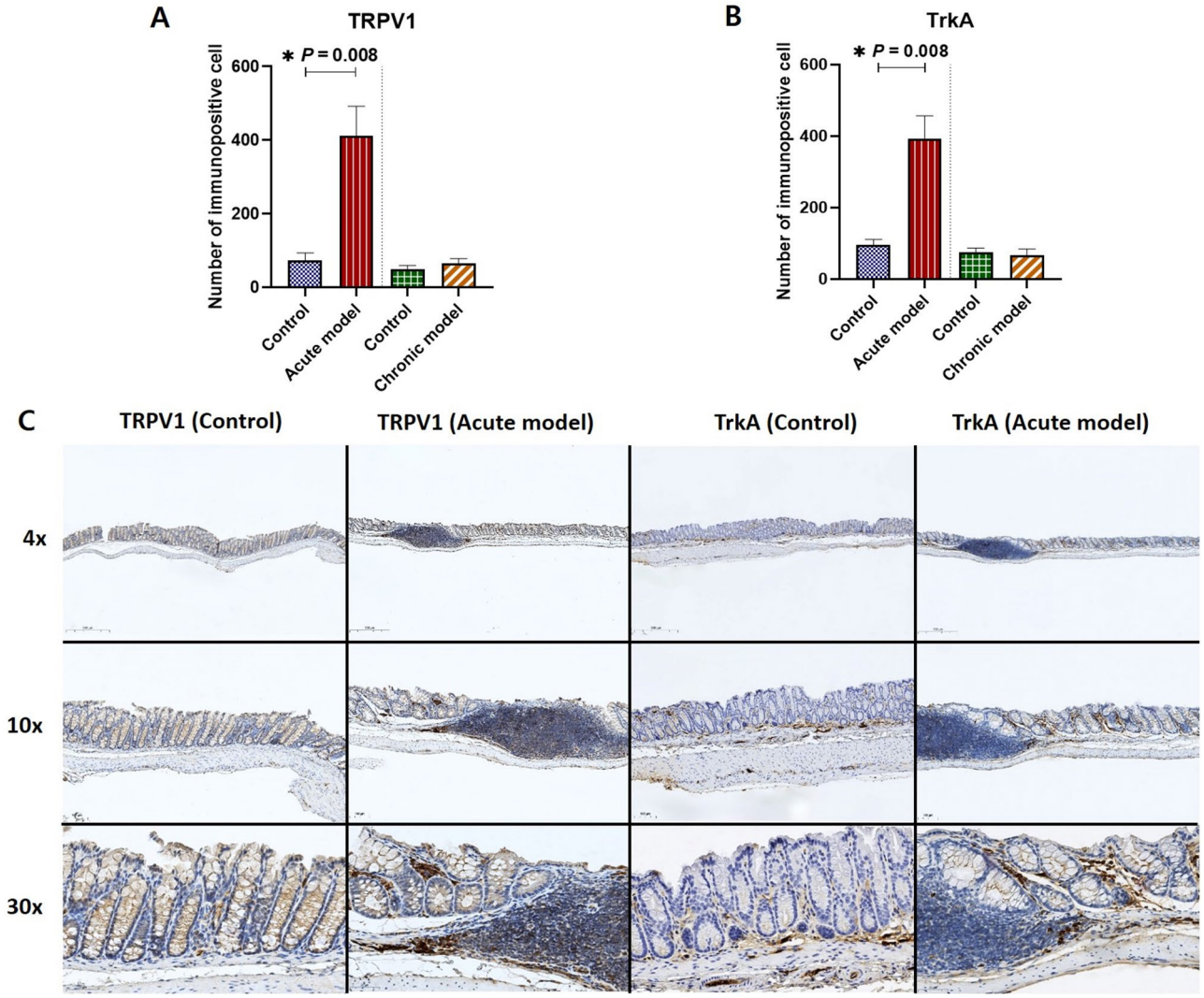

Fig. 5. Immunohistochemistry and immunohistochemical staining of neuroinflammatory markers in the irritable bowel syndrome models. (**A**,**B**) Expression of TRPV1 (**A**) and TrkA (**B**) in both models. In the acute model, TRPV1 and TrkA are quantitatively and meaningfully higher in immunopostive cells. (**C**) Immunohistochemical staining of TRPV1 and TrkA in the lamina propria and colonic epithelium of the acute model, chronic model, and control at ×4, ×10, and ×30 magnifications. Increased expression of TRPV1 and TrkA in the acute model, particularly in inflammatory cells within the epithelium and lamina propria, suggests heightened neuroinflammation and visceral hypersensitivity. In contrast, the chronic model showed minimal expression of these markers. Strong brown staining indicates high marker expression, while light blue or brown staining was common across all groups. *TRPV1* transient receptor potential vanilloid 1, *TrkA* tropomyosin receptor kinase A.

In comparison to various previous IBS animal models[5], the stress-induced chronic visceral pain model has been commonly utilized. However, these models could pose ethical limitations due to the use of physical stressors like restraint, water avoidance, and neonatal-maternal separation in rodents[5,23]. Animal models of IBS with other mechanisms have been investigated, including several post-infectious IBS animal models caused by bacterial and parasitic infections such as *Campylobacter jejuni*, *Salmonella enterica*, or *Trichinella spiralis*[5,24,25]. However, since post-infectious IBS is influenced by pathogens, there is a limitation that the symptoms in murine models induced by bacterial or parasitic pathogens may differ from those of actual human post-infectious IBS[25]. On the other hand, the representative post-inflammatory IBS model using trinitrobenzene sulfonic acid has the limitation of lacking a standardized protocol regarding dosage, concentration, and administration site[25].

Therefore, a new methodology of IBS animal modeling was required. Our approach aimed to characterize a post-inflammatory IBS murine model by inducing low-grade inflammation using DSS, a method that is easily used for establishing IBS animal models[11,26]. Referring to the previous DSS-induced IBD murine model, we conducted experiments to induce low-grade inflammation by administering high concentrations of DSS for a short period or repeated low concentrations[26]. Although DSS has been used previously in IBD studies, we used DSS to induce post-inflammatory IBS due to low-grade inflammation after DSS-induced colitis. To

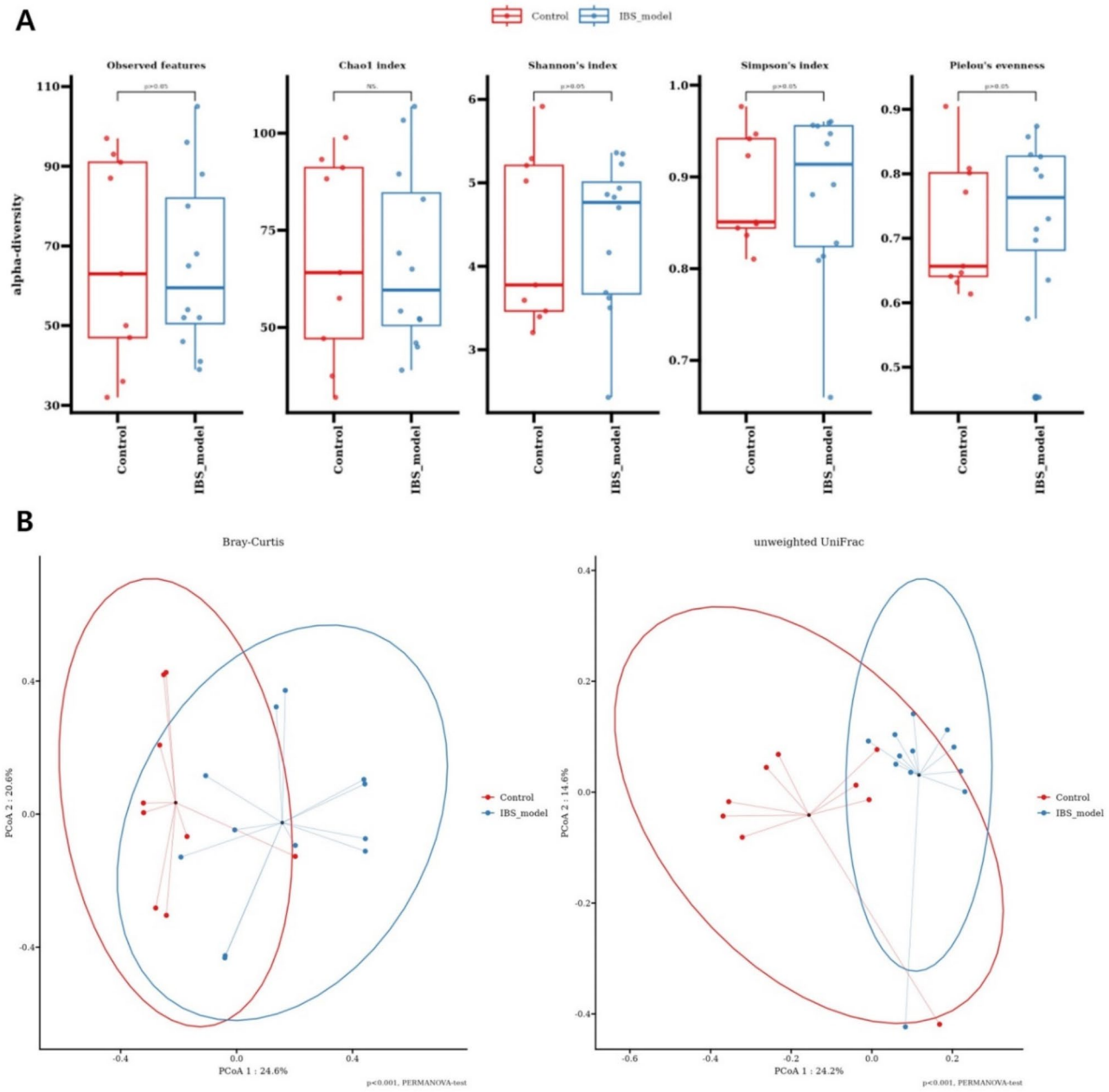

Fig. 6. Comparison of the alpha diversity and beta diversity of the microbiome between the controls and the IBS model. (**A**) Alpha diversity indices (Observed features, Chao1 index, Shannon's index, Simpson's index, and Pielou's evenness) comparing the microbiome diversity within individual samples between the control and the acute model considered as an IBS model. No significant differences were observed in alpha diversity. (**B**) Beta diversity analysis (Bray–Curtis dissimilarity and Unweighted UniFrac dissimilarity) comparing the microbiome composition between the control and the IBS model. Significant differences in beta diversity indicate distinct microbial communities between the two groups. *IBS* irritable bowel syndrome.

evaluate bowel motility changes, we measured the change in intestinal transit time *in vivo*[10]. In our IBS model, the GITT analysis using real-time CCTV showed that the transit time increased until 8 weeks after high-dose DSS administration and significantly decreased after 12 weeks compared to the controls. The distinct changes in GITT observed at week 8 suggest adaptive responses: the acute model showed shortened GITT likely due to inflammation-induced neuroinflammatory signaling and muscle contractility changes, whereas the prolonged GITT in the control group may reflect natural, age-related factors. Similar to our study, a previous study reported changes in colonic motility following recovery from alterations in the mucosal immune system[11]. Our findings also demonstrated mild leukocyte infiltration in the lamina propria in both the acute and chronic models. Because various inflammatory cytokines were elevated in the acute model compared to those in the chronic model, we speculated that low-grade inflammation in the acute model may affect the enteric immune system, leading to the

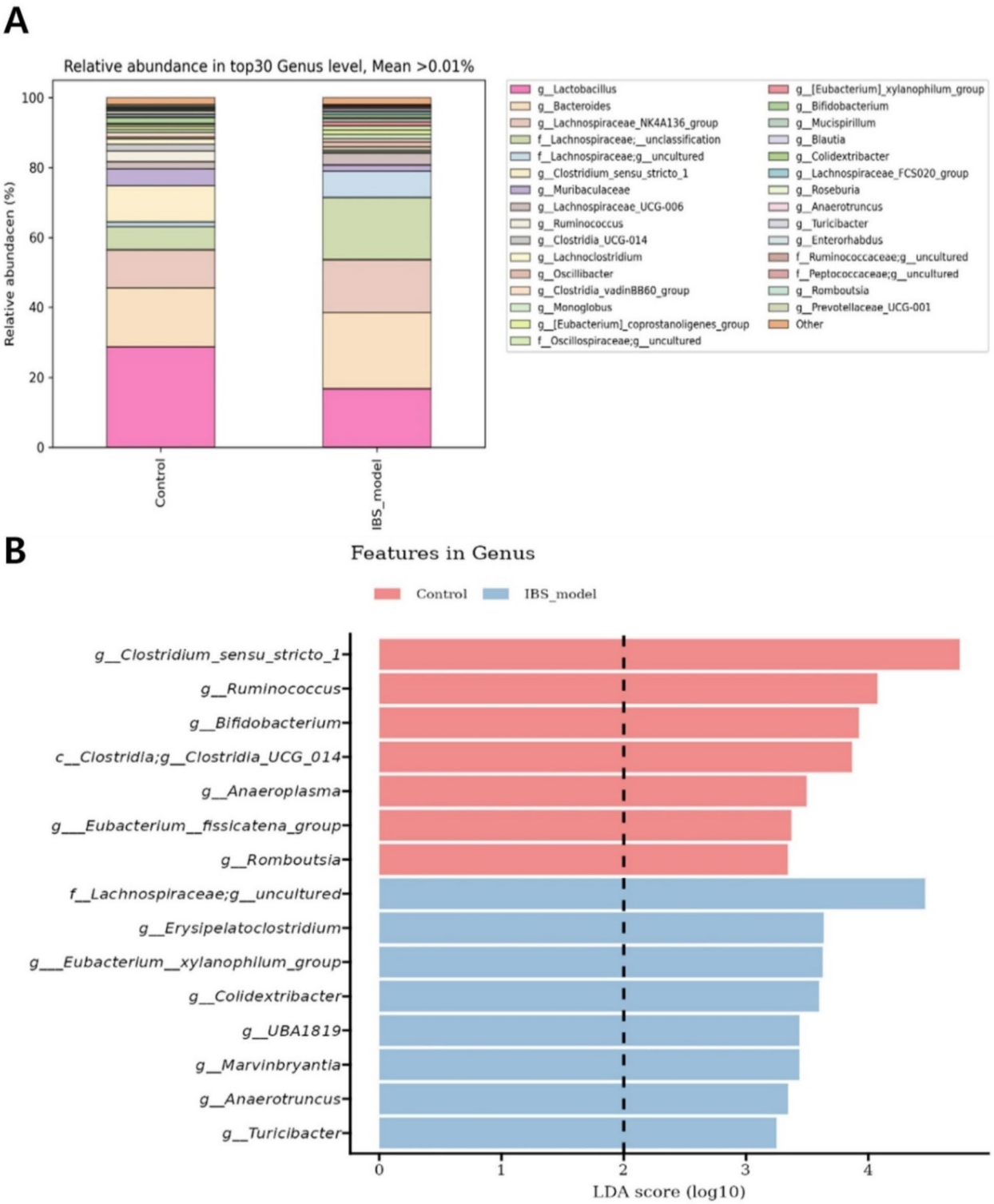

Fig. 7. Taxonomy composition analysis between the controls and the IBS model. (**A**) Relative abundance of the top 30 genera in the microbiome of the control and the acute model considered as an IBS model. (**B**) Genera with significantly different abundance between the control and IBS model. A higher abundance of genera such as *Lachnospiraceae* and *Ruminococcaceae* in the IBS model suggests their potential role in the disease's pathophysiology. *IBS* irritable bowel syndrome.

characterization of the IBS model. Additionally, we considered that the increase in IL-17 expression in the acute model, which can enhance intestinal muscle contractility, might affect colonic motility[27].

The expression of the tight junction protein occludin decreased in the proximal colon of the acute model, whereas no notable differences were observed in the chronic model. Previous studies have also reported that intestinal permeability was related to tight junction proteins, and occludin plays a major role in IBS[28,29]. Coëffier et al.[28] demonstrated that proteasome alterations enhance intestinal permeability due to decreased occludin expression in IBS. Furthermore, increased levels of IL-1β mRNA have been shown to reduce the occludin expression and increase intestinal permeability in a colitis mouse model[29]. Concordant with these studies; our study also demonstrates decreased occludin expression induced by IL-1β overexpression.

Visceral hypersensitivity is an important pathogenesis of IBS and can be induced by various pathophysiological abnormalities. To indirectly predict visceral hypersensitivity, we used IHC staining for several neuroinflammatory markers known to be associated with visceral hypersensitivity in previous studies. Previous studies have reported that TRPV1 is widely distributed in the gastrointestinal tract and plays a role in visceral hypersensitivity in IBS[30]. In a mouse model of early life stress-induced IBS, TrkA is activated and disrupts gut homeostasis, leading to dysfunction[31]. In addition, substance P, S100 protein, and NSE were over-expressed in IBS patients[5]. The IHC staining results for these markers showed that TRPV1 and TrkA immunopositivity was quantitatively higher only in the acute model. Therefore, we could indirectly predict that our IBS model might have increased visceral hypersensitivity.

Several studies have suggested that microbial alterations are critical in the pathogenesis of IBS. In our acute post-inflammatory IBS model, we observed a significant increase in the abundance of genera such as *Lachnospiraceae* and *Ruminococcaceae*, suggesting a different microbial composition compared to controls. This finding is consistent with previous research by Jeffery et al.[32], which showed that *Lachnospiraceae* can disrupt the mucosal barrier. Such disruption may increase intestinal permeability in IBS patients. In addition, *Ruminococcaceae* are known to produce short-chain fatty acids, which play a role in modulating visceral hypersensitivity, a key feature of IBS pathophysiology[33]. These microbial imbalances likely contribute to IBS symptoms by affecting gut motility, barrier function, and sensitivity. Furthermore, while alpha diversity did not show significant differences, beta diversity analysis revealed distinct microbial communities between the IBS model and controls. This suggests that specific shifts in microbial composition, rather than overall diversity, may be key to IBS pathogenesis. Our findings of increased *Lachnospiraceae* and *Ruminococcaceae* are similar to those of previous studies that have associated these genera with immune activation and changes in intestinal permeability that may exacerbate IBS symptoms[1]. While further research is needed to clarify the precise role of these microbial groups in IBS pathogenesis, our findings can provide a foundation for exploring microbiome dynamics and their impact on gut health.

In our model research on IBS utilizing the post-inflammatory model, several strong points have been observed. First, this model effectively mirrors altered gastrointestinal motility function and post-inflammatory visceral hypersensitivity, closely reflecting the post-inflammatory symptoms of IBS observed in humans. This aspect is particularly valuable, given that low grade-inflammatory states are a critical factor in IBS pathogenesis. Second, although visceral hypersensitivity may decrease over time, the post-inflammatory model accurately replicates the resolution of acute enteritis and chronic healing phase, making it suitable for modeling the chronic natural course of IBS. Furthermore, pilot studies have established experimental conditions, such as the dosage and duration of inflammatory agents, to induce a consistent level of inflammation, thus ensuring reproducibility of results. On the other hand, certain limitations remain. First, this model does not currently address mechanisms involving brain-gut interactions, such as psychological stress, which are integral to IBS pathogenesis in humans. Moving forward, we will consider integrating psychological stress paradigms with our existing model to more accurately simulate the multifactorial nature of IBS. Second, we did not investigate the effect of gender differences in our model. Third, in investigating the pathophysiology of human IBS including visceral hypersensitivity or increased intestinal permeability, surrogate markers such as TRPV1 and occludin expression were employed. However, future studies would benefit from incorporating methods such as barostat assessments, Fluorescein isothiocyanate-dextran assays, or *in vivo* tracer methods to provide more comprehensive mechanistic insights.

In conclusion, this study characterized DSS-induced low-grade inflammation in an acute recovery model following severe colitis. The findings revealed key physiological changes, including gut dysmotility, altered permeability, increased visceral hypersensitivity, and notable shifts in microbial composition, without overt colonic damage. This model provides a valuable tool to study the multifactorial mechanisms underlying IBS, particularly the role of inflammation and microbiome alterations. Our experimental models hold promise for diverse IBS studies, allowing for future investigations of pathophysiological mechanisms and targeted therapies.

Data availability

The datasets used and/or analyzed in the current study are available from the corresponding author on reasonable request.

Received: 3 July 2024; Accepted: 3 February 2025
Published online: 12 March 2025

References

1. Holtmann, G. J., Ford, A. C. & Talley, N. J. Pathophysiology of irritable bowel syndrome. *Lancet Gastroenterol. Hepatol.* **1**, 133–146 (2016).
2. Black, C. J. & Ford, A. C. Global burden of irritable bowel syndrome: trends, predictions and risk factors. *Nat. Rev. Gastroenterol. Hepatol.* **17**, 473–486 (2020).

3. Drossman, D. A. Functional gastrointestinal disorders: history, pathophysiology, clinical features, and Rome IV. *Gastroenterology* **150**, 1262–1279 (2016). e1262.
4. JohnBritto, J. S. et al. Gender-specific insights into the irritable bowel syndrome pathophysiology. Focus on gut dysbiosis and permeability. *Eur. J. Intern. Med.* (2024).
5. Wang, Y. et al. Rodent model of irritable bowel syndrome. *Int. J. Gastroenterol. Disord. Ther.* **4**, 131 (2017).
6. Moloney, R. D., O'Mahony, S. M., Dinan, T. G. & Cryan, J. F. Stress-induced visceral pain: toward animal models of irritable-bowel syndrome and associated comorbidities. *Front. Psychiatry*. **6**, 15. https://doi.org/10.3389/fpsyt.2015.00015 (2015).
7. Long, Y., Liu, Y., Tong, J., Qian, W. & Hou, X. Effectiveness of trimebutine maleate on modulating intestinal hypercontractility in a mouse model of postinfectious irritable bowel syndrome. *Eur. J. Pharmacol.* **636**, 159–165. https://doi.org/10.1016/j.ejphar.2010.03.037 (2010).
8. Piccione, M. et al. STW 5 herbal preparation modulates Wnt3a and Claudin 1 gene expression in zebrafish IBS-like model. *Pharmaceuticals* **14**, 1234 (2021).
9. Halpin, S. J. & Ford, A. C. Prevalence of symptoms meeting criteria for irritable bowel syndrome in inflammatory bowel disease: systematic review and Meta-analysis. *Off. J. Am. Coll. Gastroenterol. ACG.* **107**, 1474–1482. https://doi.org/10.1038/ajg.2012.260 (2012).
10. Chassaing, B., Aitken, J. D., Malleshappa, M. & Vijay-Kumar, M. Dextran sulfate sodium (DSS)-induced colitis in mice. *Curr. Protoc. Immunol.* **104**, 15.25.11–15.25.14. https://doi.org/10.1002/0471142735.im1525s104 (2014).
11. Kodani, M. et al. Association between gastrointestinal motility and macrophage/mast cell distribution in mice during the healing stage after DSS-induced colitis. *Mol. Med. Rep.* **17**, 8167–8172 (2018).
12. Ito, R. et al. Interferon-gamma is causatively involved in experimental inflammatory bowel disease in mice. *Clin. Exp. Immunol.* **146**, 330–338. https://doi.org/10.1111/j.1365-2249.2006.03214.x (2006).
13. Li, Z. et al. Essential roles of enteric neuronal serotonin in gastrointestinal motility and the development/survival of enteric dopaminergic neurons. *J. Neurosci.* **31**, 8998–9009 (2011).
14. Kishi, K., Kamizaki, M., Kaji, N., Iino, S. & Hori, M. A close relationship between networks of interstitial cells of Cajal and gastrointestinal transit in vivo. *Front. Pharmacol.* **11**, 587453 (2020).
15. Turner, J. R., Buschmann, M. M., Romero-Calvo, I., Sailer, A. & Shen, L. In *Seminars in Cell & Developmental Biology.* 204–212 (Elsevier).
16. Erben, U. et al. A guide to histomorphological evaluation of intestinal inflammation in mouse models. *Int. J. Clin. Exp. Pathol.* **7**, 4557 (2014).
17. Luo, C. et al. Upregulation of the transient receptor potential vanilloid 1 in colonic epithelium of patients with active inflammatory bowel disease. *Int. J. Clin. Exp. Pathol.* **10**, 11335 (2017).
18. Bukin, Y. S. et al. The effect of 16S rRNA region choice on bacterial community metabarcoding results. *Sci. Data*. **6**, 1–14 (2019).
19. Bolyen, E. et al. Reproducible, interactive, scalable and extensible microbiome data science using QIIME 2. *Nat. Biotechnol.* **37**, 852–857 (2019).
20. Callahan, B. J. et al. DADA2: high-resolution sample inference from Illumina amplicon data. *Nat. Methods*. **13**, 581–583 (2016).
21. Weinstein, M. M., Prem, A., Jin, M., Tang, S. & Bhasin, J. M. FIGARO: An efficient and objective tool for optimizing microbiome rRNA gene trimming parameters. *bioRxiv*. 610394 (2019).
22. Chang, F., He, S. & Dang, C. Assisted selection of biomarkers by linear discriminant analysis effect size (LEfSe) in microbiome data. *JoVE (J. Vis. Exp.)*. e61715 (2022).
23. Greenwood-Van Meerveld, B., Prusator, D. K. & Johnson, A. C. Animal models of gastrointestinal and liver diseases. Animal models of visceral pain: pathophysiology, translational relevance, and challenges. *Am. J. Physiol.-Gastrointest. Liver Physiol.* **308**, G885–G903 (2015).
24. Beatty, J. K., Bhargava, A. & Buret, A. G. Post-infectious irritable bowel syndrome: mechanistic insights into chronic disturbances following enteric infection. *World J. Gastroenterol. WJG*. **20**, 3976 (2014).
25. Qin, H. Y. et al. Systematic review of animal models of post-infectious/post-inflammatory irritable bowel syndrome. *J. Gastroenterol.* **46**, 164–174 (2011).
26. Perše, M. & Cerar, A. Dextran sodium sulphate colitis mouse model: traps and tricks. *J. Biomed. Biotechnol.* **2012** (2012).
27. Andoh, A., Ogawa, A., Bamba, S. & Fujiyama, Y. Interaction between interleukin-17-producing CD4+T cells and colonic subepithelial myofibroblasts: what are they doing in mucosal inflammation? *J. Gastroenterol.* **42**, 29–33 (2007).
28. Coëffier, M. et al. Increased proteasome-mediated degradation of occludin in irritable bowel syndrome. *Off. J. Am. Coll. Gastroenterol. ACG*. **105**, 1181–1188 (2010).
29. Rawat, M. et al. IL1B increases intestinal tight junction permeability by up-regulation of MIR200C-3p, which degrades occludin mRNA. *Gastroenterology* **159**, 1375–1389 (2020).
30. Choi, N. R. et al. Study on the Therapeutic effects and mechanisms of gintonin in irritable bowel syndrome and its relationship with TRPV1, TRPV4, and NaV1. 5. *Pharmaceuticals* **17**, 1170 (2024).
31. Wong, H. L. X. et al. Early life stress disrupts intestinal homeostasis via NGF-TrkA signaling. *Nat. Commun.* **10**, 1745 (2019).
32. Jeffery, I. B., Quigley, E. M., Öhman, L. & Simrén, M., O'Toole, P. W. The microbiota link to irritable bowel syndrome: an emerging story. *Gut Microbes*. **3**, 572–576. https://doi.org/10.4161/gmic.21772 (2012).
33. Pozuelo, M. et al. Reduction of butyrate-and methane-producing microorganisms in patients with irritable bowel syndrome. *Sci. Rep.* **5**, 12693 (2015).

Acknowledgements

This study was supported by a KSNM grant of the Korean Society of Neurogastroenterology and Motility for 2022.

Author contributions

E.S.J., H.K.J.: research conceptualization, experimental methodology, experiment, data analysis, drafting of the manuscript; E.S.J., H.K.J., A.Y.L., Y.S.K.: review and editing of the manuscript; E.O.C.: pathologic analysis and review; K.E.Y., Y.S.K.: microbiome experiment and analysis. All authors reviewed the manuscript.

Declarations

Competing interests

The authors declare no competing interests.

Additional information

Supplementary Information The online version contains supplementary material available at https://doi.org/1

0.1038/s41598-025-88981-7.

Correspondence and requests for materials should be addressed to H.-K.J.